Published in final edited form as:
Inorg Chem. 2008 July 7; 47(13): . doi:10.1021/ic800048e.

Synthesis, Structure, and Physical Properties for a Series of Monomeric Iron(III) Hydroxo Complexes with Varying Hydrogen-Bond Networks

Jhumpa Mukherjee[†], **Robie L. Lucas**[‡], **Matthew K. Zart**[‡], **Douglas R. Powell**[‡], **Victor W. Day**[‡], and **A. S. Borovik**[*,†]

Departments of Chemistry, University of California, Irvine, 1102 Natural Science II, Irvine, California 92697, and University of Kansas, 2010 Malott Hall, 1251 Wescoe Hall Drive, Lawrence, Kansas 66045

Abstract

Mononuclear iron(III) complexes with terminal hydroxo ligands are proposed to be important species in several metalloproteins, but they have been difficult to isolate in synthetic systems. Using a series of amidate/ureido tripodal ligands, we have prepared and characterized monomeric $Fe^{III}OH$ complexes with similar trigonal-bipyramidal primary coordination spheres. Three anionic nitrogen donors define the trigonal plane, and the hydroxo oxygen atom is trans to an apical amine nitrogen atom. The complexes have varied secondary coordination spheres that are defined by intramolecular hydrogen bonds between the $Fe^{III}OH$ unit and the urea NH groups. Structural trends were observed between the number of hydrogen bonds and the $Fe–O_{hydroxo}$ bond distances: the more intramolecular hydrogen bonds there were, the longer the Fe–O bond became. Spectroscopic trends were also found, including an increase in the energy of the O–H vibrations with a decrease in the number of hydrogen bonds. However, the $Fe^{III/II}$ reduction potentials were constant throughout the series (∼2.0 V vs $[Cp_2Fe]^{0/+1}$), which is ascribed to a balancing of the primary and secondary coordination-sphere effects.

Introduction

Iron complexes with terminal hydroxo ligands have been implicated in a variety of biological processes. Reactive monomeric $Fe^{III}OH$ complexes are proposed in the catalytic cycles of several non-heme iron oxygenases,[1] whereby the hydroxo ligand is generated from the activation of O_2. Stable monomeric $Fe^{III}OH$ complexes have also been observed within the active sites of metalloproteins such as iron superoxide dismutase[2] and lipoxygenase.[3] In these systems, there are intramolecular hydrogen bonds (H-bonds) between the hydroxo ligand and the species present in the secondary coordination sphere. Studies on these proteins have shown that modifying H-bond networks affects the structural and physical properties of the $Fe^{III}OH$ complexes, which ultimately are linked to functional changes.

There are few analogous synthetic Fe^{III} complexes with terminal hydroxo ligands because of the propensity of hydroxide ions to bridge between metal ions.[4] Our group[5] and others[6–8] have shown that placing the hydroxo ligand within a H-bonding cavity allows for the

[*]To whom correspondence should be addressed. aborovik@uci.edu.
[†]University of California, Irvine.
[‡]University of Kansas.

Supporting Information **Available:** CIFs for the X-ray experiments on $K[Fe^{III}\mathbf{0}^{iPr}(OH)]\cdot DMF$ and $K[Fe^{III}H\mathbf{1}^{iPr}(OH)]\cdot 1.5Et_2O$. This material is available free of charge via the Internet at http://pubs.acs.org.

isolation of monomeric MOH complexes. However, we are aware of only a single study, one that involved $Zn^{II}OH$ complexes, that examined the effects of varying H-bonds on the structural and physical properties of metal–hydroxo species.[8] We recently introduced a series of amidate/ureido tripodal ligands that create cavities with varied H-bonding networks when coordinated to a metal ion.[9] The ligands are all trianionic, resulting from monodeprotonation of the amide or urea groups that are present on each tripodal arm. The urea groups have an additional NH group that serves as an H-bond donor, allowing for modulation of the number of intramolecular H-bonds within a series of complexes having similar primary coordination spheres.

In this report, we describe the preparation and properties of the first series of $Fe^{III}OH$ complexes with tunable H-bond networks (Figure 1). The complexes are prepared from the Fe^{II} complexes with oxidants, including O_2. Our results demonstrate that there are correlations between H-bond networks and the structural, spectroscopic, and electrochemical properties of the complexes.

Experimental Section

Preparative Methods and Syntheses

All reagents were purchased from commercial sources and used as received, unless otherwise noted. Solvents were sparged with argon and dried over columns containing Q-5 and a molecular sieve. Anhydrous solvents were purchased from Aldrich (Milwaukee, WI). Potassium hydride (KH) as a 30% dispersion in mineral oil was filtered with a medium-porosity glass frit, washed five times each with pentane and Et_2O, dried under vacuum, and stored under an inert atmosphere. Trimethylamine *N*-oxide was purified by sublimation. The syntheses of the ligands and their intermediates were carried out under a dinitrogen atmosphere. Dioxygen was dried on a Drierite gas purifier, which was purchased from Fisher Scientific. 9,10-Dihydroanthracene (DHA) was recrystallized three times from EtOH and dried under vacuum. The syntheses of all metal complexes were conducted in a Vacuum Atmospheres Co. (Hawthorne, CA) drybox under an argon atmosphere. Elemental analyses were accomplished at Desert Analytics (Tucson, AZ). The preparation of $H_3\mathbf{0}^{iPr}$, $H_4\mathbf{1}^{iPr}$, $H_5\mathbf{2}^{iPr}$, H_6buea, and $K[Fe^{III}H_3buea(OH)]$ followed literature proce-dures.[5,9]

Syntheses with Trimethylamine *N*-Oxide (Me_3NO). Potassium {Bis[(*N′-tert*-butylureayl)-*N*-ethyl](*N″*-isopropylcarbamoylmethyl) aminato(hydroxo)ferrate(III)}, $K[Fe^{III}H_2\mathbf{2}^{iPr}(OH)]$

A solution of the ligand $H_5\mathbf{2}^{iPr}$ (100 mg, 0.250 mmol) dissolved in anhydrous dimethylacetamide (DMA; 4 mL) was treated with solid KH (30 mg, 0.75 mmol). The mixture was stirred until gas evolution ceased. $Fe(OAc)_2$ (43 mg, 0.25 mmol) was added to the pale-yellow solution, and stirring was continued for 30 min. The mixture was filtered to remove KOAc (45 mg, 92% for 2 equiv) and the resulting amber filtrate treated with Me_3NO (19 mg, 0.25 mmol). The dark-red-orange solution was stirred for 1 h, filtered to remove a small amount of insoluble material, and then concentrated in vacuo. The residue was mostly redissolved with CH_3CN and filtered. Vapor diffusion of Et_2O into the filtrate produced a dark-red-orange solid, which was filtered, washed with Et_2O, and dried under vacuum to 100 mg (79%). Anal. Calcd (found) for $K[Fe^{III}H_2\mathbf{2}^{iPr}(OH)]$, $C_{19}H_{38}FeKN_6O_4$: C, 44.79 (45.08); H, 7.52 (7.20); N, 16.49 (16.16). FTIR (Nujol, cm^{-1}) ν(OH) 3668/3670, ν(NH) 3252/32, ν(CO) 1586, 1549. λ_{max} (DMA; nm (ε, M^{-1} cm^{-1})): 376 (5300).

Potassium {[(*N′-tert*-butylureayl)-*N*-ethyl]bis(*N″*-isopropylcarbamoylmethyl)aminato(hydroxo)ferrate(III)}, $K[Fe^{III}H1^{iPr}$-(OH)], was prepared using the same procedure as that for $K[Fe^{III}H_2\mathbf{2}^{iPr}(OH)]$ with $H_4\mathbf{1}^{iPr}$ (100 mg, 0.280 mmol), KH (34 mg, 0.85 mmol), $Fe(OAc)_2$ (49 mg, 0.28 mmol), and Me_3NO (21 mg,

0.28 mmol) to afford 105 mg (81%) of the product. Vapor diffusion of Et_2O into the reaction mixture produced crystals suitable for structural analysis by X-ray diffraction. Anal. Calcd (found) for $K[Fe^{III}H\mathbf{1}^{iPr}(OH)]$, $C_{17}H_{33}FeKN_5O_4$: C, 43.78 (43.81); H, 7.13 (7.00); N, 15.01 (15.12). FTIR (Nujol, cm^{-1}): ν(OH) 3676, ν(NH) 3248, ν(CO) 1588, 1550. λ_{max} (DMA, nm (ε, M^{-1} cm^{-1})): 346 (sh), 374 (5300).

Potassium {Tris[(*N* -isopropylcarbamoylmethyl)aminato(hydroxo)ferrate(III)}, $K[Fe^{III}\mathbf{0}^{iPr}(OH)]$

A solution of the ligand $H_3\mathbf{0}^{iPr}$ (100 mg, 0.317 mmol) dissolved in anhydrous DMA (4 mL) was treated with solid KH (38 mg, 0.95 mmol). The mixture was stirred until gas evolution ceased. $Fe(OAc)_2$ (55 mg, 0.32 mmol) was added to the pale-yellow solution, and stirring was continued for 1 h. The mixture was filtered to remove KOAc (45 mg, 92% for 2 equiv), and DHA (29 mg, 0.16 mmol) or 1,2-diphenylhydrazine (DPH; 29 mg, 0.16 mmol) was added under magnetic stirring. The resulting amber filtrate was treated with Me_3NO (24 mg, 0.32 mmol), and the yellowish-brown solution was stirred for 1 h. After concentration of the reaction mixture to dryness under vacuum, the residue was redissolved in *N*,*N*-dimethylformamide (DMF). Vapor diffusion of Et_2O resulted in a yellow solid that was filtered, washed with Et_2O, and dried under vacuum to give 100 mg (79%) of the product. Anal. Calcd (found) for $K[Fe^{III}H_2\mathbf{0}^{iPr}(OH)]$, $C_{15}H_{28}FeKN_4O_4$: C, 42.85 (42.56); H, 6.57 (6.67); N, 13.03 (13.23). FTIR (Nujol, cm^{-1}): ν(OH) 3692, ν(NH) 3176, ν(CO) 1581. λ_{max} (DMA, nm (ε, M^{-1} cm^{-1})): 376 (5300).

Syntheses with O_2. $K[Fe^{III}H_2\mathbf{2}^{iPr}(OH)]$

A DMF solution (4 mL) of $H_5\mathbf{2}^{iPr}$ (100 mg, 0.250 mmol) was treated with solid KH (30 mg, 0.75 mmol), and the mixture was stirred until gas evolution ceased. $Fe(OAc)_2$ (43 mg, 0.25 mmol) was then added to the pale-yellow solution, and stirring was continued for 30 min. The mixture was filtered to remove KOAc and the amber filtrate treated with dry O_2 (3.04 mL, 0.125 mmol, T = 22 °C, P = 757 torr) via syringe. The dark-red-orange solution was stirred for 1 h and then concentrated in vacuo. The residue was mostly redissolved with CH_3CN and filtered. Vapor diffusion of Et_2O into the filtrate produced a dark-red-orange solid, which was filtered, washed with Et_2O, and dried under vacuum to give 102 mg (80%) of the product. Spectroscopic properties of the dark-red-orange solid prepared by this method are the same as those of the dark-red-orange solid prepared with Me_3NO.

$K[Fe^{III}H\mathbf{1}^{iPr}(OH)]$ was prepared with O2 following the procedure outlined above for $K[Fe^{III}H_2\mathbf{2}^{iPr}(OH)]$ with $H_4\mathbf{1}^{iPr}$(100. mg, 0.279 mmol), KH (30 mg, 0.85 mmol), $Fe(OAc)_2$ (43 mg, 0.28 mmol), and dry O_2 (3.4 mL, 0.14 mmol, T = 24 °C, P = 755 torr) to afford 94 mg (72%) of $K[Fe^{III}H\mathbf{1}^{iPr}(OH)]$. The analytical and spectroscopic properties matched those of the salt obtained with Me_3NO.

$K[Fe^{III}\mathbf{0}^{iPr}(OH)]$

A solution of the ligand $H_3\mathbf{0}^{iPr}$ (100 mg, 0.317 mmol) dissolved in 4 mL of anhydrous DMA was treated with solid KH (38 mg, 0.95 mmol). The mixture was stirred until gas evolution ceased. $Fe(OAc)_2$ (56 mg, 0.32 mmol) was added to the pale-yellow solution, and stirring was continued for 1 h. The mixture was filtered to remove KOAc (45 mg, 92% for 2 equiv), and DPH (29 mg, 0.16 mmol) was added to it under magnetic stirring. The reaction mixture was treated with dry O_2 (3.9 mL, 0.16 mmol, T = 21 °C, P = 757 torr) via syringe. The dark-brown reaction mixture changed color to yellowish orange during the 1 h stirring time. The excess O_2 was removed from the reaction mixture, and it was then concentrated in vacuo. The crude solid was dissolved in DMF and filtered to remove the insoluble solid. Vapor diffusion of Et_2O into the DMF solution resulted in a yellow solid that was filtered, washed

with Et_2O, and dried under vacuum to give 95 mg (71%) of the product. Spectroscopic properties of the yellow solid match those of the product obtained by other methods.

Physical Measurements

NMR spectra were recorded on a Bruker Avance 400 MHz spectrometer equipped with a Silicon Graphics workstation. Fourier transform infrared (FTIR) spectra were collected on a Mattson Genesis series or on a Varian 800 Scimitar series FTIR instrument with values reported in wavenumbers. Perpendicular-mode electron paramagnetic resonance (EPR) spectra were collected using a Bruker EMX spectrometer equipped with an ER041XG microwave bridge. Spectra for EPR samples were collected using the following spectrometer settings: attenuation = 25 dB, microwave power = 0.638 mW, frequency = 9.64 GHz, sweep width = 5000 G, modulation amplitude = 10.02 G, gain = 1.00×10^3, conversion time = 81.920 ms, time constant = 655.36 ms, and resolution = 1024 points. Low-temperature (4 K) spectra were obtained using an Oxford Instruments liquid-helium quartz cryostat. Cyclic voltammetric experiments were conducted using a CHI600C electrochemical analyzer following methods previously described.[10] A 1.0 mm glassy carbon or 1.0 mm Pt electrode was used as the working electrode to measure the cyclic voltammograms (CVs) at scan velocities between 0.1 and 1.0 V/s. A ferrocinium/ferrocene couple ($[Cp_2Fe]^{+/0}$) was used to monitor the reference electrode (Ag^+/Ag), which was observed at $E_{1/2}$ = 0.245 V with ΔE_p = 0.090 V and $i_{pa} \cdot i_{pc}^{-1}$) 0.82 at an ν = 0.1 V/s in DMA at ambient temperature.

X-ray Crystallographic Data Collection and Refinement of the Structures

Intensity data for $K[Fe^{III}\mathbf{0}^{iPr}(OH)]$, $K[Fe^{III}H\mathbf{1}^{iPr}(OH)]$, and $K[Fe^{III}H_2\mathbf{2}^{iPr}(OH)]$ were collected using a Bruker APEX CCD area detector[11] mounted on a Bruker D8 goniometer using graphite-monochromated Mo Kα radiation (λ = 0.710 73 Å). The sample was cooled to 100(2) K. The intensity data, which nominally covered one and half hemispheres of reciprocal space, were measured as a series of ω oscillation frames each of 0.3° for 30 s/frame. The detector was operated in 512 × 512 mode and was positioned 5.054 cm from the sample. Coverage of unique data was 99.4% complete to 26.00° in θ. The structures were solved by direct methods and refined by full-matrix least-squares methods on F^2. Hydrogen atom positions were initially determined by geometry and refined by a riding model. Non-hydrogen atoms were refined with anisotropic displacement parameters. Hydrogen atom displacement parameters were set to 1.2 (1.5 for methyl) times the displacement parameters of the bonded atoms. The displacement ellipsoids were drawn at a 50% probability level. The data were corrected for absorption by the semiempirical method. Space groups were determined by statistical methods and verified by subsequent refinement. Partial crystal data, data collection, and refinement parameters for $K[Fe^{III}\mathbf{0}^{iPr}(OH)] \cdot DMF$ and $K[Fe^{III}H\mathbf{1}^{iPr}(OH)] \cdot 1.5Et_2O$ are listed in Table 1.

$K[Fe^{III}\mathbf{0}^{iPr}(OH)]\cdot DMF$ crystallized in the triclinic space group $P\bar{1}$ with cell parameters determined from a nonlinear least-squares fit of 4029 peaks in the range $2.29° < \theta < 26.00°$. A total of 10 999 data were measured in the range $2.23° < \theta < 26.00°$. Minimum and maximum transmission factors of 0.7079 and 0.9094 were used in the absorption correction. A total of 282 parameters were refined against 4888 data to give $wR(F^2)$ = 0.1603 and S = 1.018 for weights of $w = 1/[\sigma^2(F^2) + (0.0960P)^2 + 1.6000P]$, where $P = [F_o^2 + 2F_c^2]/3$. The final $R(F)$ was 0.0547 for the 4077 observed, $[F > 4\sigma(F)]$, data. The largest shift/su was 0.019 in the final refinement cycle. The final difference map had maxima and minima of +0.868 and −0.397 e/Å^3, respectively.

$K[Fe^{III}H\mathbf{1}^{iPr}(OH)]\cdot 1.5Et_2O$ crystallized in the monoclinic space group $C2/c$ with cell parameters determined from a nonlinear least-squares fit of 6342 peaks in the range $2.29° <$

$\theta < 26.00°$. The determination was made by systematic absences and statistical tests and verified by subsequent refinement. A total of 19 294 data were measured in the range $2.23° < \theta < 26.00°$. The first 50 frames were repeated at the end of data collection and yielded a total of 465 peaks, showing a variation of 0.18% during the data collection. The data were corrected for absorption by the semiempirical method,[12] giving minimum and maximum transmission factors of 0.8017 and 0.9309. The data were merged to form a set of 6080 independent data with $R(\text{int}) = 0.0212$. A total of 463 parameters were refined against 230 restraints and 6080 data to give $wR(F^2) = 0.0831$ and $S = 1.020$ for weights of $w = 1/[\sigma^2(F^2) + (0.0480P)^2 + 5.8000P]$, where $P = [F_o^2 + 2F_c^2]/3$. The final $R(F)$ was 0.0300 for the 5609 observed, $[F > 4\sigma(F)]$, data. The largest shift/su was 0.001 in the final refinement cycle. The final difference map had maxima and minima of +0.524 and −0.472 e/Å^3, respectively. The unique part of the unit cell contains one potassium, one metal complex, and one and a half solvent molecules. One side arm of the metal complex, O2, N3, C9–C12, was disordered and modeled in two orientations with occupancies refined to 0.58(4) and 0.42(4) for the unprimed and primed atoms. The solvent in a general position, (S), was disordered and refined in two orientations with occupancies refined to 0.539(4) and 0.461(4). The other solvent, (T), sits on a crystallographic 2-fold axis. All atoms of the (T) solvent were refined with a fixed occupancy of 0.5. Restraints on the positional and displacement parameters of the disordered and solvent atoms were required. The displacement parameters of C9 and C9′ were set to be equal.

K[Fe^{III}H$_2$**2**^{iPr}(OH)] crystallizes in the space group $P2_1/c$ with unit cell dimensions of a = 11.4612(18) Å, b = 20.669(3) Å, c = 27.010(4) Å, $\alpha = 90°$, $\beta = 90.359(3)°$, and $\gamma = 90°$. Unfortunately, the crystals obtained diffracted weakly, giving a low yield of quality data and producing a solution with R1 = 14%.

Results and Discussion

Preparation of the Complexes

The syntheses of [Fe^{III}H$_2$**2**^{iPr}(OH)]$^-$ and [Fe^{III}H**1**^{iPr}(OH)]$^-$ were accomplished by oxidation of their respective Fe^{II} precursors with either Me$_3$NO or O$_2$, which we have used in the past to prepare [Fe^{III}H$_3$buea(OH)]$^-$.[5b] In a typical reaction, deprotonation of H$_5$**2**^{iPr} with 3 equiv of KH in DMA, followed by treatment of the resulting mixture with Fe(OAc)$_2$, gave a pale-amber mixture from which 2 equiv of KOAc was removed by filtration. The resulting filtrate was treated with Me$_3$NO to produce a dark-red-orange solution, with K[Fe^{III}H$_2$**2**^{iPr}(OH)] being obtained in 79% yield following isolation and recrystallization of the crude product from CH$_3$CN. For oxidation reactions with molecular oxygen, a DMA solution of [Fe^{II}H$_2$**2**^{iPr}]$^-$ was treated with 0.5 equiv of O$_2$, producing a dark-red-orange solution containing K[Fe^{III}H$_2$**2**^{iPr}(OH)], which was isolated in 80% recrystallized yield.

The final member of this series utilized the deprotonated amide ligand [**0**^{iPr}]$^{3-}$, a ligand framework that does not contain H-bond donors. We have found that the best yields of [Fe^{III}**0**^{iPr}(OH)]$^-$ occurred when external substrates with relatively weak C–H bonds were present in the reaction mixture. For example, treating a solution of [Fe^{III}**0**^{iPr}]$^-$ with either DHA or DPH prior to the addition of oxidant produced the yellow [Fe^{III}**0**^{iPr}(OH)]$^-$ complex and oxidized organic products (anthracene or azobenzene) in yields approaching 80%. Note that the reactivity observed for [Fe^{III}**0**^{iPr}]$^-$ differs from the other complexes in this series that do not require additional reagents to obtain good yields of Fe^{III}OH product. A more detailed structure–function analysis on the various Fe^{II} precursors will be described in a forthcoming account.

The isolation of [Fe^{III}**0**^{iPr}(OH)]$^-$ completed a series of related monomeric Fe^{III}OH complexes that were designed to have similar primary coordination spheres yet differing

microenvironments surround the $Fe^{III}OH$ units (Figure 1). The complexes should have varying numbers of intramolecular H-bonds that are formed between the urea NH groups of the tripodal ligands and the hydroxo oxygen atom. We were therefore for the first time able to examine systematically the effects of different H-bond networks on the structural and physical properties of metal hydroxo complexes.

Structural Studies

The solid-state molecular structures for the iron(III) hydroxo complexes, obtained for their respective potassium salts, were studied by single-crystal X-ray diffraction techniques. Thermal ellipsoid plots of $[Fe^{III}H\mathbf{1}^{iPr}(OH)]^-$ and $[Fe^{III}\mathbf{0}^{iPr}(OH)]^-$ are shown in Figure 2, and selected metrical parameters are listed in Table 2. We have reported previously the molecular structure of $[Fe^{III}buea(OH)]^-$;[5b] thus, its properties will only be discussed in comparison to those of the other complexes. The obtained model for the molecular structure of $[Fe^{III}H_2\mathbf{2}^{iPr}(OH)]^-$ is consistent with a monomeric $Fe^{III}OH$ complex with trigonal-bipyramidal (TBP) coordination geometry. However, the low quality of the data allowed us to give only a qualitative assessment of the structure, which prevented comparisons with the other complexes.

The molecular structures revealed that each complex is five-coordinated with TBP coordination geometry. The deprotonated urea (αN^-)/amide nitrogen atoms defined the trigonal planes in each complex. The similar Fe1–$N_{amid/urea}$ bond distances found throughout the series of complexes indicated that deprotonated amides and ureas are capable of providing comparable primary coordination spheres around a metal ion. For instance, in $[Fe^{III}\mathbf{0}^{iPr}(OH)]^-$, containing three deprotonated amide donors, the Fe1—N_{amid} bond distances are statistically identical, with an average value of 2.022(2) Å. At the other end of the series, the in-plane donors of $[Fe^{III}H_3buea(OH)]^-$ consist solely of monodeprotonated ureas, and the average Fe1—N_{urea} bond distance is 2.016 (2) Å. There is a slightly greater spread in Fe1— $N_{amid/urea}$ distances for hybrid complex $[Fe^{III}H\mathbf{1}^{iPr}(OH)]^-$, in which the iron–ureido nitrogen bond distance (Fe1—N2) is the shortest at 2.002(1) Å, with the two Fe —N_{amid} bonds (i.e., Fe1–N3 and Fe1–N4) being significantly longer at 2.013(1) and 2.031(1) Å, respectively.

The apical amine nitrogen atom, N1, of the tripodal ligands occupies one of the axial coordination positions in each complex. The other axial position is taken up by the exogenous hydroxo ligand. The hydroxo oxygen atom, O4, is nearly trans to N1 with N1—Fe1—O4 angles greater than 177°. The hydroxo ligand in each complex sits within a cavity formed by the appropriate tripodal ligand. For complexes with urea donors, the $\alpha'N$—H groups are pointed into the cavity toward the hydroxo ligand, forming intramolecular H-bonds. All $\alpha'N\cdots O4$ distances are less than 3.0 Å (Table 2), which are within the range normally associated with H-bonds.[13] Note that broadened N—H vibrational bands in the FTIR spectra lend further support to the presence of intramolecular H-bonds in these complexes.

This series of complexes has the expected intramolecular H-bond networks that differ by the number of H-bonds. For instance, a single H-bond is present in $[Fe^{III}H\mathbf{1}^{iPr}(OH)]^-$, with an N5…O4 distance of 2.794 Å, a distance that is slightly shorter than the average $\alpha'N\cdots O4$ distance of 2.838(3) Å found in $[Fe^{III}H_3buea(OH)]^-$.[5b] The differences in the secondary coordination sphere appear to correlate with other metrical parameters within the series. A small trend is observed for the Fe1—$O_{hydroxo}$ bond distances, in which the Fe1—O4 bond distance increases as the number of H-bond donors in the ligand increases. The longest Fe1 —O4 bond distance of 1.926(2) Å is found in $[Fe^{III}H_3buea(OH)]^-$, which contains three intramolecular H-bonds. $[Fe^{III}H\mathbf{1}^{iPr}(OH)]^-$, with one H-bond, has an Fe1—O4 bond length of 1.886(1) Å, while this bond distance is shortest at 1.877(3) Å in $[Fe^{III}\mathbf{0}^{iPr}(OH)]^-$. In

addition, a similar trend is found for the displacement of the iron center from the trigonal plane. Each iron is positioned out of the trigonal plane, away from N1. The greatest displacement of 0.432 Å is seen in $[Fe^{III}\mathbf{0}^{iPr}(OH)]^-$, the complex without intramolecular H-bonds. The other distances shorten with an increase in the H-bonds: 0.405 Å in $[Fe^{III}H\mathbf{1}^{iPr}(OH)]^-$ and 0.338 Å in $[Fe^{III}H_3buea(OH)]^-$.

The $Fe–O_{hydroxo}$ bond distances in this series compare well to those reported in other systems having intramolecular H-bonds. An Fe–O distance of 1.876(2) Å was found for a six-coordinate, monomeric $Fe^{III}OH$ complex having intramolecular H-bonds to the oxygen atom of the hydroxo ligand.[7] In addition, a porphyrin-based system has been reported that produces a secondary coordination sphere with a single H-bond donor around the $Fe^{III}OH$ unit to produce an $Fe–O_{hydroxo}$ bond of 1.868 Å.[14] Finally, iron superoxide dismutase contains an iron hydoxo center that is TBP and has an $Fe–O_{hydroxo}$ bond length of 1.994 Å. This protein system also has multiple H-bonds formed between the hydroxo ligand and the amino acid residues present in the active site.[15]

In a previous report, we showed that in $[Fe^{III}H_3buea(OH)]^-$ the O–H bond is positioned between two of the urea arms of the $[H_3buea]^{3-}$ ligand,[5b] causing a widening of one of the trigonal-plane angles to greater than 128° (Table 2). This type of distortion in the trigonal plane is not observed in the other complexes, which have in-plane bond angles ranging from 114.5(4) to 117.5(4)° in $[Fe^{III}H\mathbf{1}^{iPr}(OH)]$ and from 113.7(1) to 117.8(1)° in $[Fe^{III}\mathbf{0}^{iPr}(OH)]^-$. The amidate-containing complexes appear to have less constrained cavities, resulting in the O–H vector being positioned within the cavities, toward a methine carbon atom of one of the appended isopropyl groups. This orientation of the hydroxo ligands does not require large distortions within the trigonal plane, as is observed when the O–H vector is positioned outward, between two arms of the tripodal ligand.

Spectroscopic Properties

A variety of spectroscopy methods were used to further explore the effects of intramolecular H-bonds on the properties of the $Fe^{III}OH$ units. FTIR spectroscopy was used to analyze the energies of the O–H vibrations, which were found to decrease as the number of H-bonds increased. The O–H vibration for $[Fe^{III}\mathbf{0}^{iPr}(OH)]^-$, having no hydrogen bond, is seen at the highest energy at ν(O–H) = 3690 cm^{-1}. $[Fe^{III}H\mathbf{1}^{iPr}(OH)]^-$ contains only a single H-bond, and its O–H stretch is at 3676 cm^{-1}. The O–H vibration of $[Fe^{III}H_2\mathbf{2}^{iPr}(OH)]^-$ is observed at 3668 cm^{-1}, whereas in $[Fe^{III}H_3buea(OH)]^-$, which contains the greatest number of H-bonds, it occurs at the lowest energy at 3632 cm^{-1}. This trend is expected because H-bonds remove electron density from the $Fe^{III}OH$ unit through the oxygen atom, which, in turn, weakens both the Fe^{III}–O and O–H bonds.

A trend is observed in the UV-vis absorption spectra for DMA solutions of the iron(III) hydroxo complexes. For instance, $[Fe^{III}\mathbf{0}^{iPr}(OH)]^-$ has λ_{max} = 346 nm, which we have tentatively assigned to a charge-transfer transition based on its large extinction coefficent (~5000 M^{-1} cm^{-1}). The complexes with one and two intramolecular H-bonds, $[Fe^{III}H\mathbf{1}^{iPr}(OH)]^-$ and $[Fe^{III}H_2\mathbf{2}^{iPr}(OH)]^-$, have nearly identical values of 374 and 376 nm, respectively. $[Fe^{III}H_3buea(OH)]^-$ absorbs at the lowest energy, with a λ_{max} of 398 nm. Thus, the energies of the absorption bands decrease with an increase in the number of H-bonds. This trend is opposite to that observed in a series of copper(II) azido complexes for absorbance bands assigned as ligand-to-metal charge trans-fer.[16] It is presently unclear as to why opposite trends were observed.

The complexes were further probed using EPR spectroscopy: the spectra for $[Fe^{III}H_2\mathbf{2}^{iPr}(OH)]^-$, $[Fe^{III}H\mathbf{1}^{iPr}(OH)]^-$, and $[Fe^{III}\mathbf{0}^{iPr}(OH)]^-$, recorded at 4 K in perpendicular mode, are shown in Figure 3. The spectral features are similar to those

reported for [$Fe^{III}H_3$buea(OH)] and are consistent with high-spin iron centers.[5b] The temperature dependencies of the spectra indicate that complexes have the same zero-field-splitting parameter of −1.3 cm^{-1}; therefore, the observed signals arise from excited-state doublets. Similar rhombic splitting parameters (*E*/*D*) were also obtained, with values ranging from 0.17 to 0.11 (Table 3). These findings mirror the structural results, which found distortions in the ligand fields around the Fe^{III} ions. Several factors contribute to the distorted ligand geometries, including the coordination of the hydroxo ligands within the cavity and the inherent rhombic ligand fields caused by the hybrid ligands. Note that [$Fe^{III}H_3$buea(OH)]$^-$ had the largest *E*/*D* value, even though it has a symmetrical tripodal ligand, which is attributed to the greater angular distortions within the trigonal plane.

Electrochemical Properties

The electrochemical properties of the complexes were investigated using cyclic voltammetry (Table 3); Figure 4 shows the CVs for [$Fe^{III}H_2$**2**^{iPr}(OH)]$^-$, [Fe^{III}H**1**^{iPr}(OH)]$^-$, and [Fe^{III}**0**^{iPr}(OH)]$^-$ recorded as DMA solutions using a platinum working electrode. The complexes with urea donors undergo one-electron-reduction processes that are assigned to the $Fe^{III/II}$OH couples. These reductions are quasi-reversible under the scan velocity tested and occur at nearly the same potentials, which are centered around −1.9 V vs $[Cp_2Fe]^{0/+1}$. The symmetrically amidate complex [Fe^{III}**0**^{iPr}(OH)]$^-$ has an irreversible reduction at E_{pc} = −1.94 V vs $[Cp_2Fe]^{0/+}$, a value that is comparable to those found for the other complexes in the series (Table 3).

The similarities in redox potentials for the Fe^{III}OH complexes are counter to what have been reported for most other systems with varied H-bond networks, in which a positive shift in the potential is associated with an increase in the number of H-bonds to the coordinated ligand(s).[17] This correlation is rationalized as a stabilization of the reduced species owning to the H-bonds weakening the ligand field around the metal center(s). However, it is well recognized that the electronic effects of the tripodal ligands also influence redox potentials. For instance, our previous work on four-coordinate, monopyramidal Co^{II} complexes with the same set of tripodal ligands found a correlation between redox potentials and the number of ureido donors: the Co^{II} oxidation potentials shifted negatively as the number of ureido donors increased.[9] A similar trend in the Fe^{III}OH complexes would be expected if the redox potentials were governed solely by the primary coordination sphere. However, there are varying numbers of intramolecular H-bonds involving the hydroxo ligands in the Fe^{III}OH complexes. Therefore, as the number of urea donors increases (favoring negative potentials), there is a concomitant increase in the number of H-bonds to the hydroxo ligand, which should cause a positive shift in the potential. It is thus possible that these two effects are offsetting, producing the nearly constant values for the Fe^{III}OH reduction.

Summary

We have described the preparation of a series of monomeric Fe^{III}OH complexes by reacting Fe^{II} precursors with oxidants, including O_2. The Fe^{III}OH complexes have similar TBP primary coordination spheres, with the terminal hydroxo ligand positioned within cavities created by a series of amidate/ureido tripodal ligands. The cavities have varied numbers of H-bond donors that interact with the hydroxo ligand and affect the structural and physical properties of the complexes. Trends in structural, vibrational, electronic, and electrochemical properties were observed for the complexes, which are ascribed to the differing H-bond networks surrounding the Fe^{III}OH units. These results further emphasize the importance of controlling the secondary coordination sphere around metal complexes.

Supplementary Material

Refer to Web version on PubMed Central for supplementary material.

Acknowledgments

We thank the NIH (Grant NIH50781) for financial support and the NSF (Grant CHE-0079282) for funding the X-ray diffraction instrumentation. We thank Professor Mike Hendrich for determining the EPR parameters.

References

1. (a) Hausinger RP. Crit Biochem Mol Biol. 2004; 39:21–68.(b) Costas M, Mehn MP, Jensen MP, Que L Jr. Chem Rev. 2004; 104:939–986. [PubMed: 14871146]
2. (a) Yikilmaz E, Xie J, Brunold TC, Miller AF. J Am Chem Soc. 2002; 124:3482–3483. [PubMed: 11929218] (b) Xie J, Yikilmaz E, Miller AF, Brunold TC. J Am Chem Soc. 2002; 124:3769–3774. [PubMed: 11929267] (c) Lah MS, Dixon MM, Pattridge KA, Stallings WC, Fee JA, Ludwig ML. Biochemistry. 1995; 34:1646–1660. [PubMed: 7849024] (d) Jackson TA, Brunold TC. Acc Chem Res. 2004; 37:461–470. [PubMed: 15260508] (e) Yikilmaz E, Rodgers DW, Miller AF. Biochemistry. 2006; 45:1151–1161. [PubMed: 16430211] (f) Yikilmaz E, Porta J, Grove LE, Vahedi-Faridi A, Bronshteyn Y, Brunold TC, Borgstahl GEO, Miller AF. J Am Chem Soc. 2007; 129:9927–9940. [PubMed: 17628062]
3. (a) Tomchick DR, Phan P, Cymborowski M, Minor W, Holman TR. Biochemistry. 2001; 40:7509–7517. [PubMed: 11412104] (b) Schenk G, Neidig ML, Zhou J, Holman TR, Solomon EI. Biochemistry. 2003; 42:7294–7302. [PubMed: 12809485]
4. (a) Que L Jr, Tolman WB. Angew Chem, Int Ed. 2002; 41:1114–1137.(b) Kurtz DM Jr. Chem Rev. 1990; 90:585–606.
5. (a) MacBeth CE, Hammes BS, Young VG Jr, Borovik AS. Inorg Chem. 2001; 40:4733–4741. [PubMed: 11511223] (b) MacBeth CE, Gupta R, Mitchell-Koch KR, Young VG Jr, Lushington GH, Thompson WH, Hendrich MP, Borovik AS. J Am Chem Soc. 2004; 126:2556–2567. [PubMed: 14982465]
6. Berreau LM, Mahapatra S, Halfen JA, Young VG Jr, Tolman WB. Inorg Chem. 1996; 35:6339.
7. Ogo S, Wada S, Watanabe Y, Iwase M, Wada A, Harata M, Jitsukawa K, Masuda H, Einage H. Angew Chem, Int Ed. 1998; 37:2102–2104.
8. (a) Mareques Rivas JC, Prabaharan R, de Rosales RTM. Chem Commun. 2004; 7:6–77.(b) Mareques Rivas JC, Salvagni E, Parsons S. Chem Commun. 2004:460–461.(c) Mareques Rivas JC, de Rosales RTM, Parsons S. Chem Commun. 2004:610–611.(d) Mareques Rivas JC, Prabaharan R, Parsons S. Dalton Trans. 2004:1648–1655. [PubMed: 15252616] (e) Feng G, Mareque-Rivas JC, de Rosales RTM, Williams NH. J Am Chem Soc. 2005; 127:13470–13471. [PubMed: 16190690]
9. Lucas RL, Muhkerjee J, Zart MK, Sorrell TN, Powell DR, Borovik AS. J Am Chem Soc. 2006; 128:15476–15489. [PubMed: 17132015]
10. Ray M, Hammes BS, Yap GPA, Rheingold Liable-Sands L, Borovik AS. Inorg Chem. 1998; 37:1527–1533.
11. (a) Data Collection: SMART Software Reference Manual. Bruker-AXS; Madison, WI: 1994. (b) Data Reduction: SAINT Software Reference Manual. Bruker-AXS; Madison, WI: 1995.
12. Sheldrick, GM. SADABS: Program for Empirical Absorption Correction of Area Detector Data. University of Göttingen; Göttingen, Germany: 2000.
13. (a) Jeffrey, GA. An Introduction to Hydrogen Bonding. Oxford University Press, Inc.; New York: 1997. (b) Desiraju, GR.; Steiner, T. The Weak Hydrogen Bond in Structural Chemistry and Biology. Oxford University Press Inc.; New York: 1999.
14. Yeh CY, Chang CJ, Nocera DG. J Am Chem Soc. 2001; 123:1513–1514. [PubMed: 11456732]
15. Lah MS, Dixon MM, Pattridge KA, Stallings WC, Fee JA, Ludwig ML. Biochemistry. 1995; 34:1646–1660. [PubMed: 7849024]
16. Wada A, Honda Y, Yamaguchi S, Nagatomo S, Kitagawa T, Jitsukawa K, Masuda H. Inorg Chem. 2004; 43:5725–5735. [PubMed: 15332825]

17. (a) Mareque Rivas JC, Hinchley SL, Metteau L, Parsons S. Dalton Trans. 2006:2316–2322. [PubMed: 16688319] (b) Suzuki N, Higuchi T, Urano Y, Kikuchi K, Uekusa H, Ohashi Y, Uchida T, Kitagawa T, Nagano T. J Am Chem Soc. 1999; 121:11571–11572.(c) Tani F, Matsu-ura M, Nakayama S, Ichimura M, Nakamura N, Naruta Y. J Am Chem Soc. 2001; 123:1133–1142. [PubMed: 11456666] (d) Mareque-Rivas JC, Prabaharan JC, Torres R, Prabaharan R, Torres Martin de Rosales RR, Metteau L, Parsons S. Dalton Trans. 2004:2800–2807. [PubMed: 15514768]

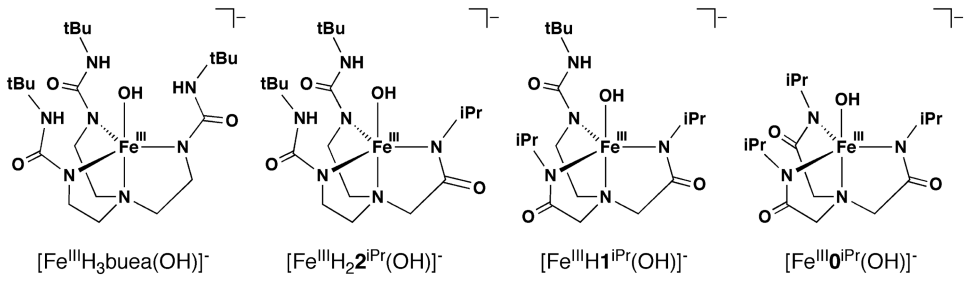

Figure 1.
$Fe^{III}OH$ complexes with varied H-bond networks used in this study.

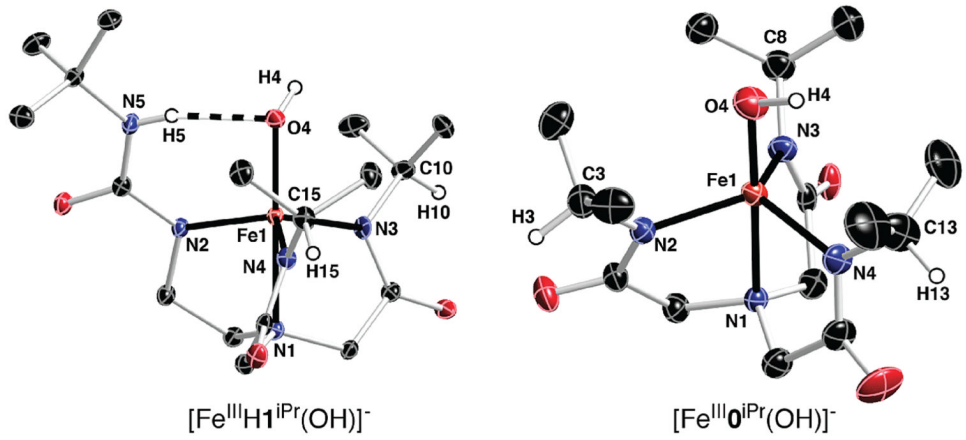

Figure 2.

Thermal ellipsoid plots illustrating the molecular structures of $[Fe^{III}H\mathbf{1}^{iPr}(OH)]^{-}$ and $[Fe^{III}\mathbf{0}^{iPr}(OH)]^{-}$. Thermal ellipsoids are drawn at the 50% level, and for clarity only urea and methine hydrogen atoms are shown. Only one of the disorder fragments containing N3 is shown for $[Fe^{III}H\mathbf{1}^{iPr}(OH)]^{-}$.

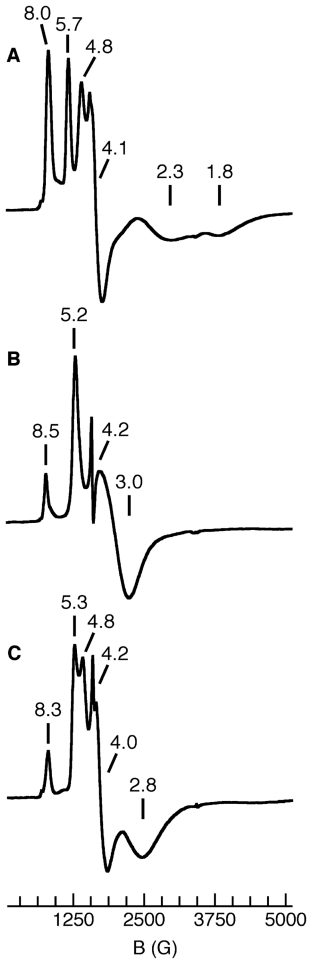

Figure 3.
X-band EPR spectra of $[Fe^{III}H_2\mathbf{2}^{iPr}(OH)]^-$ (**A**), $[Fe^{III}H\mathbf{1}^{iPr}(OH)]^-$ (**B**), and $[Fe^{III}\mathbf{0}^{iPr}(OH)]^-$ (**C**) recorded as DMA solutions at 4 K.

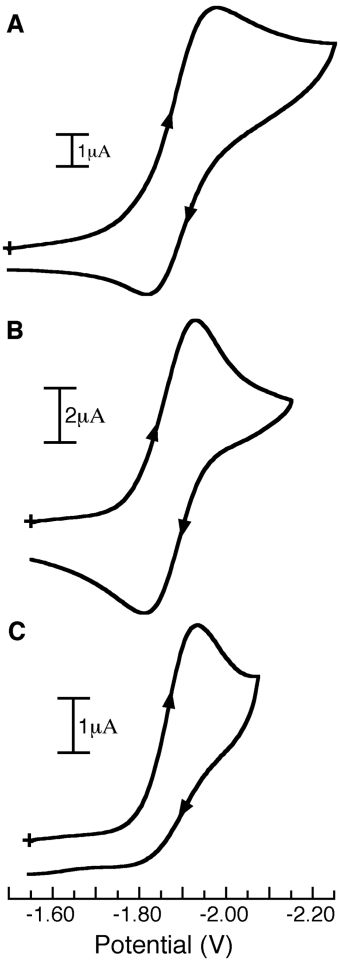

Figure 4.
CVs of $[Fe^{III}H_2\mathbf{2}^{iPr}(OH)]^-$ (**A**), $[Fe^{III}H\mathbf{1}^{iPr}(OH)]^-$ (**B**), and $[Fe^{III}\mathbf{0}^{iPr}(OH)]^-$ (**C**) recorded as DMA solutions and referenced versus $[Cp_2Fe]^{0/1+}$.

Table 1

Crystallographic Data for $K[Fe^{III}0^{iPr}(OH)] \cdot DMF$ and $K[Fe^{III}H1^{iPr}(OH)] \cdot 1.5Et_2O$

	$K[Fe^{III}0^{iPr}(OH)] \cdot DMF$	$K[Fe^{III}H1^{iPr}(OH)] \cdot 1.5Et_2O$
molecular formula	$C_{18}H_{35}FeKN_5O_5$	$C_{23}H_{46.5}FeKN_{6.5}O_{5.5}$
fw (g/mol)	496.46	597.12
T (K)	100(2)	100(2)
space group	$P1$	$C2/c$
a (Å)	9.337(3)	25.175(3)
b (Å)	10.853(4)	9.8523(12)
c (Å)	12.494(4)	26.326(3)
α (deg)	83.514(5)	90
β (deg)	86.045(5)	107.612(3)
γ (deg)	83.144(5)	90
Z	2 (Z' = 1)	8 (Z' = 1)
V (Å^3)	1247.0(7)	6223.6(13)
δ_{calcd} (Mg/m^3)	1.322	1.275
R^a	0.0547	0.0300
$R_w{}^b$	0.1603	0.0831
GOF^c	1.018	1.020

[a] $R = [\Sigma||\Delta F||\Sigma||F_O]$.

[b] $R_W = \{\Sigma[\omega(F_O{}^2 - F_C{}^2)^2]/\Sigma[\omega(F_O{}^2)^2]\}^{1/2}$.

[c] Goodness of fit on F^2.

Table 2

Selected Bond Distances and Angles for $[Fe^{III}0^{iPr}(OH)]^{-}$ and $[Fe^{III}H1^{iPr}(OH)]^{-}$

	$[Fe^{III}0^{iPr}(OH)]^{-}$	$[Fe^{III}H1^{iPr}(OH)]^{-}$
Distances (Å)		
Fe–O4	1.877(3)	1.886(1)
Fe–N1	2.194(3)	2.199(1)
Fe–N2	2.025(3)	2.002(1)
Fe–N3	2.022(3)	2.013(1)
Fe–N4	2.018(3)	2.031(1)
O4···N5		2.794(2)
Angles (deg)		
N1–Fe–O4	178.9(1)	177.70(5)
N1–Fe–N2	78.1(1)	79.29(5)
N1–Fe–N3	78.2(1)	78.1(3)
N1–Fe–N4	77.5(1)	77.13(5)
N2–Fe–N3	113.7(1)	117.5(4)
N2–Fe–N4	117.8(1)	115.79(5)
N3–Fe–N4	115.7(1)	114.5(4)
N2–Fe–O4	100.8(1)	101.69(5)
N3–Fe–O4	102.3(1)	103.2(3)
N4–Fe–O4	103.2(1)	100.58(5)

Table 3

Selected Spectroscopic and Electrochemical Results for the $Fe^{III}OH$ Complexes

	$[Fe^{III}H_3buea(OH)]^-$	$[Fe^{III}H_2{}^{2iPr}(OH)]^-$	$[Fe^{III}H1^{iPr}(OH)]^-$	$[Fe^{III}0^{iPr}(OH)]^-$
$\nu(^{16}O–H)$ (cm^{-1})	3632[a]	3668	3676	3690
λ_{max} (ε, mM^{-1} cm^{-1})	398 (4.7)[a]	376 (5.3)	374 (5.3)	346 (5.4)
D, E/D (cm^{-1})	−1.3, 0.17[a]	−1.3, 0.11	−1.3, 0.16	−1.3, 0.15
$E_{1/2}$, E_{pc}(V)[b]	−1.93 (−2.03)	−1.89 (−2.00)	−1.88 (−1.94)	c (−1.94)
ΔE_p (V)[b]	0.20	0.14	0.16	
$i_{pa}i_{pc}{}^{-1}$[b]	1.07	0.67	0.61	

[a] From ref #.

[b] Measured as DMF solutions using $[Cp_2Fe]^{0/+1}$ as the reference.

[c] Irreversible processes.